Spin dynamics in the geometrically frustrated multiferroic $CuCrO_2$

M. Poienar,[1] F. Damay,[2] C. Martin,[1] J. Robert,[2] and S. Petit[2,*]
[1]*Laboratoire CRISMAT, ENSICAEN, UMR 6508 CNRS, 6 Boulevard du Maréchal Juin, 14050 Caen Cedex, France*
[2]*Laboratoire Léon Brillouin, UMR 12, CEA-Saclay, CEA-CNRS, 91191 Gif-sur-Yvette Cedex, France*
(Received 9 December 2009; revised manuscript received 3 February 2010; published 16 March 2010)

The spin dynamics of the geometrically frustrated triangular antiferromagnet multiferroic $CuCrO_2$ have been mapped out using inelastic neutron scattering. The relevant spin Hamiltonian parameters modeling the incommensurate modulated helicoid have been determined, and correspond to antiferromagnetic nearest- and next-nearest-neighbor interactions in the *ab* plane with a strong planar anisotropy. The weakly dispersive excitation along *c* reflects the essentially two-dimensional character of the magnetic interactions. Classical energy calculations clearly point out the relevance of the balance between the adjacent planes coupling, the in-plane nearest-neighbor interactions anisotropy, and a weakly antiferromagnetic next-nearest-neighbor interaction, in stabilizing the three-dimensional magnetic order in $CuCrO_2$.

DOI: 10.1103/PhysRevB.81.104411 PACS number(s): 78.70.Nx, 75.85.+t, 75.30.Ds

I. INTRODUCTION

For more than a decade, the study of frustrated antiferromagnets has been a fascinating subject of condensed-matter physics, as the macroscopic degeneracy of the classical ground state of these systems is considered to lay the grounds for challenging novel physics. The perfect triangular lattice, an archetype for the study of geometric frustration in two dimensions (2D), has recently attracted much attention, owing to the discovery of multiferroic properties in the triangular systems delafossite oxides $CuFeO_2$ (Ref. 1) and $CuCrO_2$.[2] As shown in Fig. 1(a), these compounds are characterized at room temperature by a stacking of perfect triangular arrays, as their $R\bar{3}m$ symmetry ensures the isotropy of the in-plane couplings. Despite their inherent frustration, these systems find a way to lift their macroscopic degeneracy and to achieve a complex three-dimensional (3D) magnetic ordering below a Néel ordering temperature T_N. In the case of $CuFeO_2$ a transition from the $R\bar{3}m$ to $C2/m$ symmetry is found to accompany the magnetic ordering; this distortion is believed to help lifting the degeneracy of the frustrated magnetic lattice to achieve an Ising-type four-sublattice ($\uparrow\uparrow\downarrow\downarrow$) antiferromagnetic order at low temperature.[3–5] In $CuCrO_2$, an incommensurate magnetic structure, derived from the classical 120° spin configuration expected for a perfect planar triangular antiferromagnet,[6] has been reported.[7,8] A small magnetostriction effect, interpreted as the signature of a slight deformation of the perfect triangular lattice below T_N, has also been reported in this compound recently.[9,10] The transition to the noncollinear magnetic state in $CuCrO_2$ coincides with a ferroelectric polarization, evidencing the intimate coupling between the magnetic and electric order parameters.[11] From a microscopic point of view, the origin of this coupling remains quite puzzling, as the trigonal symmetry of these compounds imposes severe constraints on the standard theoretical models. Nonetheless, Arima[12] proposed that the polarization may actually result from a subtle modulation—a consequence of spin-orbit coupling—of the hybridization between the 3*d* cations carrying the spin and the bonding oxygen ions.

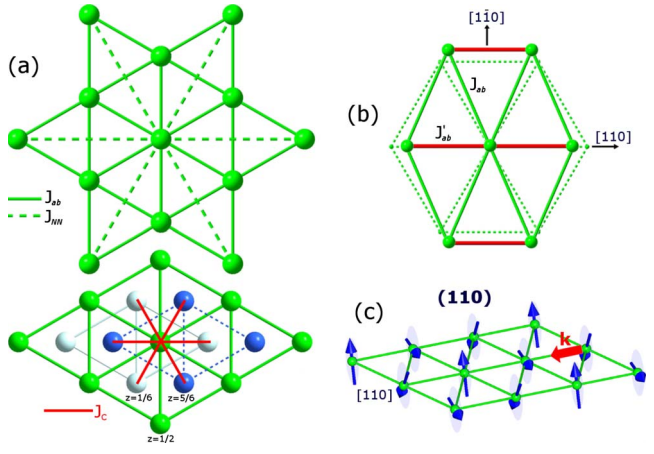

FIG. 1. (Color online) Modeling of the magnetic structure of $CuCrO_2$. (a) Illustration of the nearest-neighbor (J_{ab}) and next-nearest-neighbor (J_{NN}) magnetic interactions within the triangular plane, and between the planes (J_c) in the delafossite structure. Each Cr^{+3} is surrounded by six nearest neighbors and six next-nearest neighbors within the plane, and by 2×3 neighbors in the adjacent planes above and below. (b) Distortion of the hexagonal lattice resulting in two nearest-neighbors couplings J'_{ab} and J_{ab} according to Ref. 9. (c) Modulated helicoid with the spin-rotation axis parallel to [110]. The propagation vector is shown as a full arrow and corresponds to $\mathbf{k}=(q\ q\ 0)$ ($q\sim0.329$).

In this paper, we focus on the investigation of the magnetic couplings stabilizing the magnetic structure of $CuCrO_2$. Owing to its layered topology, significant antiferromagnetic in-plane nearest-neighbor couplings, which can be weakly anisotropic [and will be denoted J'_{ab} and J_{ab}, with $(J_{ab},J'_{ab})>0$ and $J'_{ab}>J_{ab}$, following Ref. 9, see Fig. 1(b)] is expected. Coupling between in-plane next–nearest-neighbors (J_{NN}), which has been shown to be prominent in $CuFeO_2$,[13] actually remains to be assessed in $CuCrO_2$. Interplane coupling (J_c) is, in contrast to the in-plane couplings, expected to be weak, as the rather short correlation length along the *c* axis revealed by neutron experiments[8] supports the 2D character of the compound. The helicoidal structure of $CuCrO_2$ [Fig. 1(c)] has been confirmed recently by Soda *et al.*,[14] using polarized neutron scattering, and is in agreement, in the

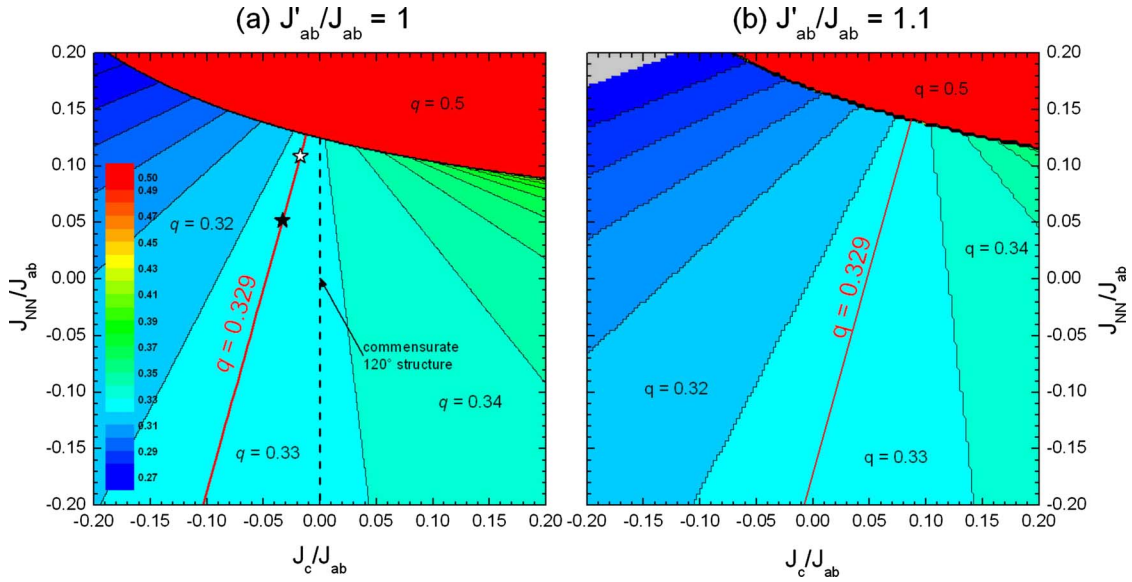

FIG. 2. (Color online) Magnetic phase diagrams in the (J_c, J_{NN}) plane of a triangular lattice with strong in-plane antiferromagnetic couplings J_{ab} and J'_{ab}, calculated for (a) $J'_{ab}/J_{ab}=1$ and (b) $J'_{ab}/J_{ab}=1.1$ (see Fig. 1 for the definition of J_{ab}, J'_{ab}, J_c, and J_{NN}). q describes the value of the propagation vector $\mathbf{k}=(q\ q\ 0)$. Stars refer to the coupling values determined in the case of the nonmodulated (empty symbol) and modulated (filled symbol) helicoidal magnetic structures.

framework of the mechanism proposed by Arima[12] with the experimentally observed ferroelectricity within the hexagonal plane.[15]

In order to study the different magnetic interactions stabilizing this helicoidal structure, we have carried out inelastic neutron scattering (INS) experiments on a single crystal of $CuCrO_2$. In parallel, we have performed energy calculations based on a standard Heisenberg model to determine the $(J_{ab}, J'_{ab}, J_{NN}, J_c)$ phase diagram of the classical ground state of $CuCrO_2$ and to investigate the influence of J'_{ab}/J_{ab}, J_{NN}, and J_c on the incommensurate deviation away from the classical 120° structure. We show that the INS data can be parametrized by a spin-wave model taking into account an easy-plane anisotropy term, a unique in-plane antiferromagnetic exchange coupling J_{ab}, and a weak next-nearest-neighbor coupling J_{NN}, which is evidenced for the first time in this compound.

II. EXPERIMENTAL METHODS

A single crystal of $CuCrO_2$ (70 mg) was grown by the flux technique, following Ref. 16. A polycrystalline sample (5 g) was also prepared according to Ref. 8. Inelastic neutron-scattering experiments were performed on the thermal (2T) and cold (4F2) neutron triple-axis spectrometers at Laboratoire Léon Brillouin (LLB)-Orphée (Saclay, France). Because of the challengingly small volume of the sample, focusing monochromators and analyzers were used to optimize the intensity, as well as standard k_f values (k_f=2.662 or 1.550 Å^{-1}) depending on the desired resolution. Higher order contaminations were removed with pyrolytic graphite or nitrogen-cooled Be filter placed in the scattered beam. The sample was mounted on an aluminum holder and aligned in the (HHL) scattering plane.

III. RESULTS

Based on a simple analysis of the magnetic structure, the properties of $CuCrO_2$ should be reasonably well described by the following spin Hamiltonian:

$$H = \sum_{i,j}^{\substack{in\\plane}} J_{ij} S_i S_j + J_c \sum_{i,j}^{\substack{inter\\plane}} S_i S_j, \qquad (1)$$

where J_{ij} are the planar exchange couplings between spins located at sites i and j on a triangular plane and correspond to nearest- (J_{ab}) and next-nearest- (J_{NN}) neighbor interactions within this triangular plane. J_c denotes the coupling between nearest neighbors in adjacent layers. Aiming at a more physical understanding of this model, we have calculated the classical energy to generate a magnetic phase diagram as a function of these different parameters (Fig. 2). To this end, the ENERMAG program[17] was used, exploring, for each point in the J space, the energy minimum, using the generalization of the Villain-Yoshimori theorem developed by Lyons and Kaplan[18] and Freiser.[19] In these calculations, we assume that the spins order with a propagation vector of the form $\mathbf{k}=(q\ q\ 0)$, as experimentally observed [this is actually confirmed to be the most stable spin configuration in a large range of J_{NN} and J_c, according to classical energy calculations searching for $\mathbf{k}$ within the (a,b) plane]. Figure 2(a) shows that in the isotropic case $(J'_{ab}/J_{ab}=1)$, if $J_c=0$, the propagation vector is $\mathbf{k}=(\frac{1}{3}\ \frac{1}{3}\ 0)$, which corresponds to the classical 120° commensurate structure. If $J_c \neq 0$, an incommensurate structure with q close to $\frac{1}{3}$ is the most stable,[20] except in the case of a strong antiferromagnetic J_{NN} coupling $(J_{NN}/J_{ab} \sim 0.1)$, which stabilizes a collinear phase with $\mathbf{k}=(\frac{1}{2}\ \frac{1}{2}\ 0)$. In the anisotropic case [illustrated in Fig. 2(b) for $J'_{ab}/J_{ab}=1.1$–note that this value was chosen arbitrarily

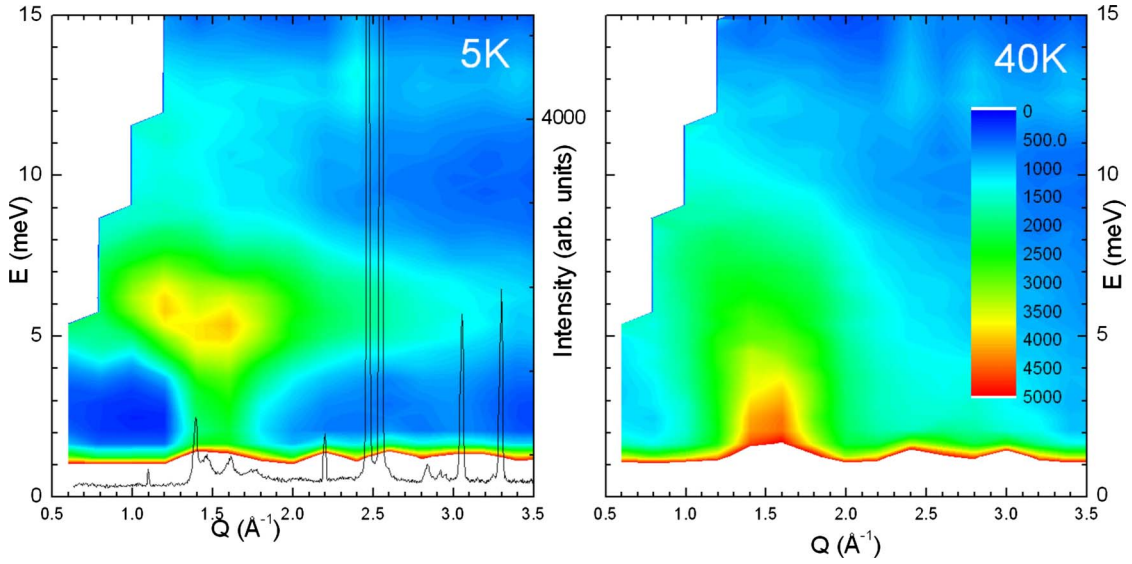

FIG. 3. (Color online) Inelastic neutron-scattering powder spectra recorded at 5 and 40 K (k_f=2.662 Å^{-1}). On the 5 K spectrum is also shown the corresponding neutron elastic scattering data (from Ref. 8).

high[10] to emphasize the effect of J'_{ab}/J_{ab} on the phase diagram], the phase diagram is shifted toward larger antiferromagnetic J_c and an incommensurate structure with $q \sim \frac{1}{3}$ is accordingly stabilized even if J_c=0. The stability range of the collinear phase is also pushed toward higher J_{NN} when $J'_{ab}/J_{ab} > 1$.

To get more insight into this problem, we have also calculated analytically the classical energy for the same $\mathbf{k}=(q\ q\ 0)$ propagation vector. The different contributions associated with subsequent neighbors are listed hereafter

$$E_{ab} = S(J'_{ab} \cos 4\pi q + 2J_{ab} \cos 2\pi q),$$

$$E_{NN} = J_{NN} S(1 + 2 \cos 6\pi q),$$

$$E_c = J_c S(1 + 2 \cos 2\pi q). \quad (2)$$

Minimizing the classical energy $E=E_{ab}+E_{NN}+E_c$ with respect to q leads to the following relation between $q(\neq 0.5)$ and J_{NN}, J_{ab}, J'_{ab}, and J_c:

$$\frac{J_c}{J_{ab}} = \frac{J_{NN}}{J_{ab}}(3 - 12 \cos^2 2\pi q) - \left(1 + 2\frac{J'_{ab}}{J_{ab}} \cos 2\pi q\right). \quad (3)$$

Equation (3) is illustrated in Fig. 2 for q=0.329 and J'_{ab}/J_{ab}=1 and 1.1. Note that if J_c is considered negligible, we find the well-known result[21]

$$\cos 2\pi q = -\frac{J_{ab}}{2J'_{ab}}, \quad (4)$$

which leads to the commensurate value $q=\frac{1}{3}$ (120° magnetic structure) in the isotropic case J'_{ab}/J_{ab}=1.

The INS measurements carried out on the powder sample give an overview of the excitation spectrum and of its temperature evolution. Figure 3 shows the neutron intensity as a function of energy and momentum transfer at 5 and 40 K. It reveals below T_N a magnetic excitation spectrum located between 1 and 9 meV, characterized by a broad maximum at ~5 meV. Because of the experimental resolution (1 meV), we cannot assert the existence of a spin gap at the Q position of the magnetic Bragg peak $(q\ q\ 0)$. The above features can be simply explained by the existence of a planar anisotropy term in the spin Hamiltonian: with this additional term, a global rotation of the spins in the easy-plane still does not cost any energy, by contrast to an out-of-plane rotation, which will cost some anisotropy energy. The spin-dynamics spectrum will have accordingly one branch having zero energy at the magnetic Bragg point (the Goldstone mode of the structure), together with other branches exhibiting a gap representative of the easy-plane anisotropy energy. In the powder average spectrum, this leads to significant scattering down to zero energy, as well as to a maximum at the energy of the gap. At T=40 K, well above T_N, the spectral weight shifts to lower energies, and significant magnetic scattering is still measured, reminiscent of short-range magnetic fluctuations.

To go further in the analysis, we carried out triple-axis experiments on a single crystal of $CuCrO_2$, in the energy range previously determined $E<9$ meV. We mapped out the magnetic excitations propagating within the hexagonal plane, along the $[H\ H\ 0]$ direction, at 10 K (Fig. 4) for k_f=1.550 and 1.97 Å^{-1} (because of the small volume of sample available, a larger k_f was employed to increase the intensity to the detriment of the instrumental resolution). The spectrum [Fig. 4(a)] can be described as follows: a main branch stems from the magnetic Bragg point $(q\ q\ 0)$ with $q \sim 0.33$. This branch does not show any clear energy gap within instrumental resolution, as is also seen on energy scans along $[\frac{1}{3}\ \frac{1}{3}\ 0]$ (not shown). However, a linear fit to the dispersion shows that if there is a gap it is actually smaller than 0.6 meV [Figs. 4(a) and 4(b)]. This branch describes an arch whose maximum reaches about 8 meV at the zone boundary $(\frac{1}{2}\ \frac{1}{2}\ 0)$ [upper red dotted line in Fig. 4(c)]. The second observable feature is weaker and is only clearly detected at high momentum, close to the zone boundary $(\frac{1}{2}\ \frac{1}{2}\ 0)$ [Fig. 4(c)]. It appears around 4

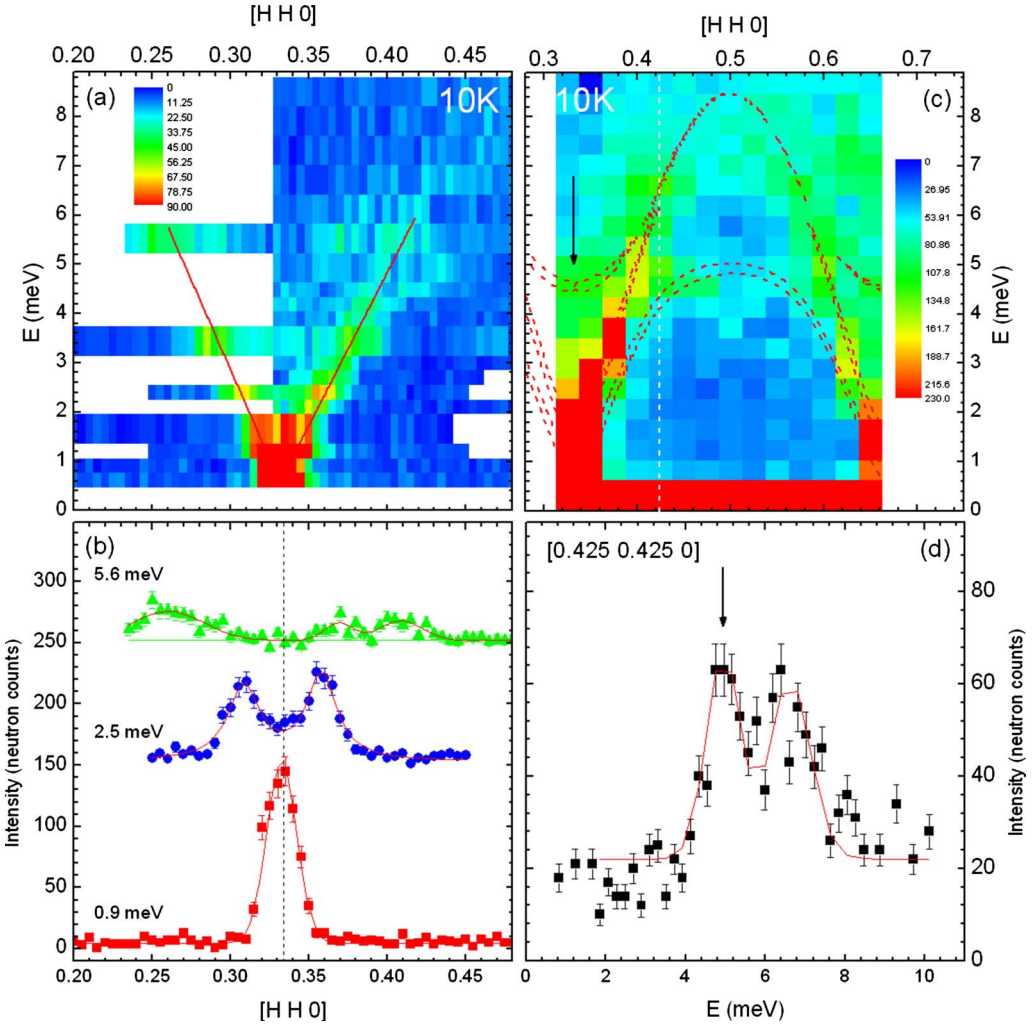

FIG. 4. (Color online) Inelastic neutron-scattering spectra at 10 K along $[H\ H\ 0]$ (k_f=1.550 Å^{-1}). (a) Spin-wave dispersion (intensity contour). Red lines are a fit to the dispersion. (b) Representative spin-wave excitation scans at constant energy transfer (E=0.9, 2.5, and 5.6 meV). Data are shifted for clarity. (c) Spin-wave dispersion (intensity contour) (k_f=1.970 Å^{-1}). (d) Constant wave-vector scans along [0.425 0.425 0] [dashed line on (c)] with k_f=1.970 Å^{-1} at 10 K. Arrows underline features described in the text.

meV and is relatively flat compared to the previous excitation, but can be clearly identified on the energy scan taken at constant Q=[0.425 0.425 0] [arrow in Fig. 4(d)]. A third feature around the zone center ($\frac{1}{3}$ $\frac{1}{3}$ 0) [shown by an arrow in Fig. 4(c)] is reminiscent of the 4 meV gap already evidenced on the powder average dispersion.

To model the spin dynamics, spin-wave calculations were performed using the SPINWAVE software developed at LLB. Based on the Holstein-Primakov approximation, the code diagonalizes any spin Hamiltonian based on Eq. (5), which is derived from Eq. (1)

$$H = J_{ab}\sum_{i,j}^{\substack{in\\plane}} S_iS_j + J_{NN}\sum_{i,j}^{\substack{in\\plane}} S_iS_j + J_c\sum_{k,l}^{\substack{inter\\plane}} S_kS_l + D_{n=(x,y,z)}\sum_i (S_in)^2. \quad (5)$$

It takes into account (isotropic or anisotropic) exchange couplings acting between neighboring spins, as well as single-ion anisotropy terms modeled by $D_{n=(x,y,z)}\Sigma_i(S_in)^2$. By definition, if D is positive, the term corresponds to an easy-plane anisotropy and n [with coordinates (x,y,z)] denotes the vector perpendicular to this plane. If D is negative, it accounts then for an easy-axis anisotropy with n being in this case the easy-axis direction. Once the spin-wave energies are known, spin-correlations functions are calculated to obtain the dynamical structure factor observed by inelastic neutron-scattering experiments. Interactions are limited to next-nearest neighbor. As the incommensurate deviation from q $=\frac{1}{3}$ is small, the calculations were made with a simplified perfect 120° spin pattern in a commensurate and perfectly triangular (J'_{ab}/J_{ab}=1) magnetic cell ($3a,3a,c$) containing 27 magnetic atoms; the (110) easy-plane, and relative spin orientations were determined according to Ref. 8 [Fig. 1(c)]. Two models were actually considered for the helicoidal magnetic structure: the first one considers that the spin-rotation envelope is circular, that is, the spin value S=1.5 is not modulated from one Cr site to the other. The second one

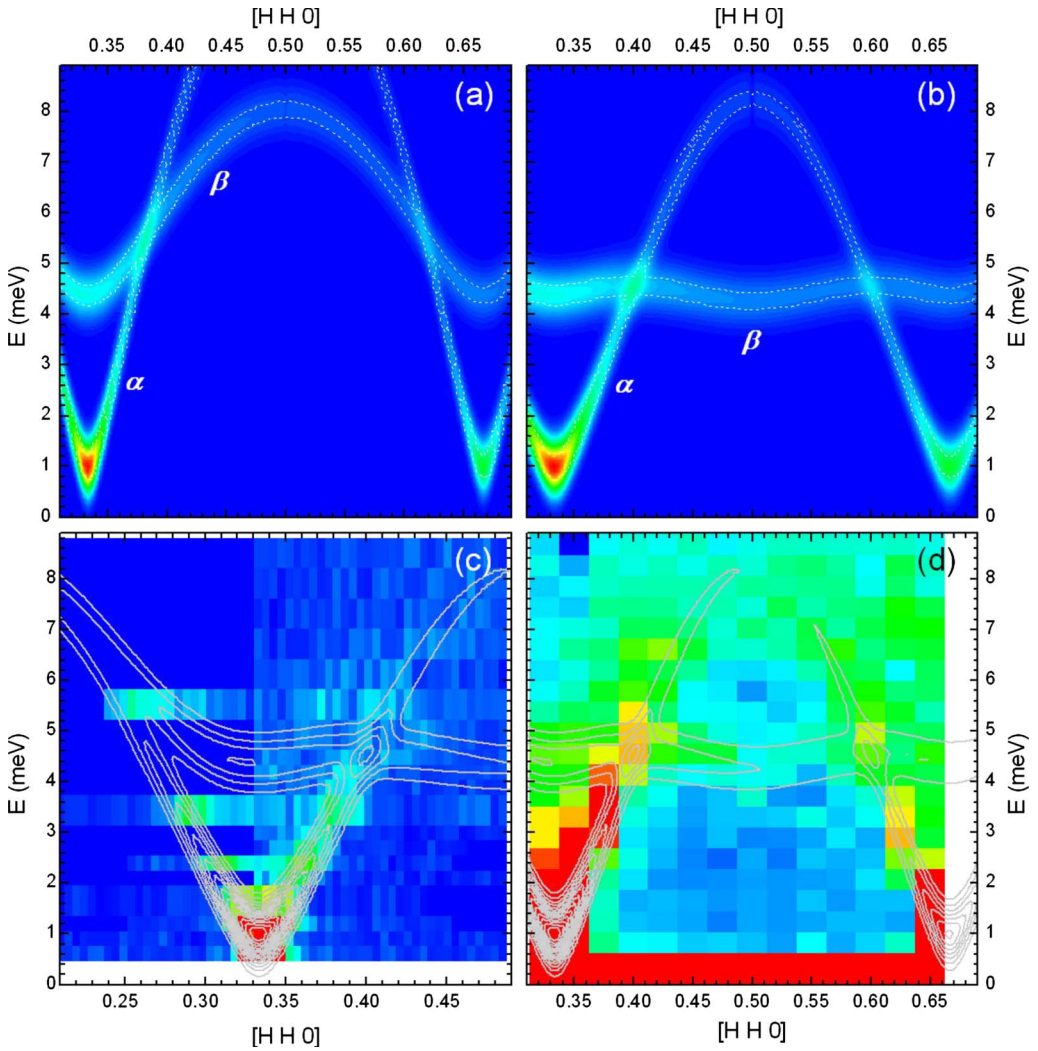

FIG. 5. (Color online) Calculated dynamical structure factor of $CuCrO_2$, plotted versus wave vector $[H\ H\ 0]$ and energy transfer E, using Heisenberg Hamiltonian (5) in the case of the nonmodulated helicoidal model (a) without J_{NN} and (b) with an additional J_{NN} coupling term (see text). The different spin-wave modes are outlined in white. [(c) and (d)] Superimposition of the calculated model (dark gray lines) on the experimental inelastic scattering data map at 10 K recorded at k_f=1.550 and 1.970 Å^{-1}, respectively.

takes into account the elliptic spin modulation described in Ref. 8, in which the spin amplitude depends on its orientation with respect to the c axis, within the easy-plane.

Figures 5 and 6 illustrate the dynamical structure factors calculated for the nonmodulated and modulated helicoidal models, respectively, as a function of the wave vector $[H\ H\ 0]$ and of the energy transfer E. In the case of the nonmodulated model, two main modes are observed, denoted ($\boldsymbol{\alpha}$) and ($\boldsymbol{\beta}$) in Fig. 5. On the experimental data, the $\boldsymbol{\beta}$ mode shows a 4 meV gap and flattens out quite quickly close to the zone boundary ($\frac{1}{2}$ $\frac{1}{2}$ 0): to describe it correctly, it is necessary to add in the modeling a small next-nearest-neighbor coupling J_{NN}, as can be seen by comparing the dispersions calculated without [Fig. 5(a)] and with antiferromagnetic next-nearest-neighbor coupling (J_{NN}=0.25 meV) [Fig. 5(b)]. As is illustrated in Figs. 5(c) and 5(d), the experimental data is accordingly best reproduced with J_{ab}=2.30 meV, J_{NN} =0.25 meV, and $D_{(110)}$=0.40 meV. The influence of interlayer coupling J_c could not be evidenced in the modeling and all the calculations were performed with J_c=0.

In the second model, which corresponds to a modulated helicoidal structure, the elliptical modulation of the spin-rotation envelope was reproduced using a spin moment S =1.4, spin parallel to [0 0 1], and two S=1.1, spin oriented at 120° and 240° with respect to [0 0 1] within the (110) plane, Fig. 1(c). This significantly affects the spin-wave dispersion: in addition to the ($\boldsymbol{\alpha_m}$) and ($\boldsymbol{\gamma_m}$) modes, another branch ($\boldsymbol{\beta_m}$), stemming from the magnetic Bragg point, is clearly observed [Fig. 6(a)]. In this case as well, it is necessary to add in the modeling a small next-nearest-neighbor coupling J_{NN}, to account for the softening of $\boldsymbol{\beta_m}$ close to the zone boundary ($\frac{1}{2}$ $\frac{1}{2}$ 0) [Fig. 6(b)]. The experimental data is here best reproduced with J_{ab}=2.30 meV, J_{NN}=0.12 meV, and $D_{(110)}$=0.40 meV, and keeping J_c=0 [Figs. 6(c) and 6(d)]. It is worth mentioning here that the zone-center energy of $\boldsymbol{\beta}$ and $\boldsymbol{\gamma_m}$ modes is approximately given by $3S\sqrt{(DJ_{ab})}$: the anisotropy term $D_{(110)}$ is thus extracted directly from the data and nearly identical for both models. As such, it can be considered, along with J_{ab}, as a fairly "robust" parameter in the modeling.

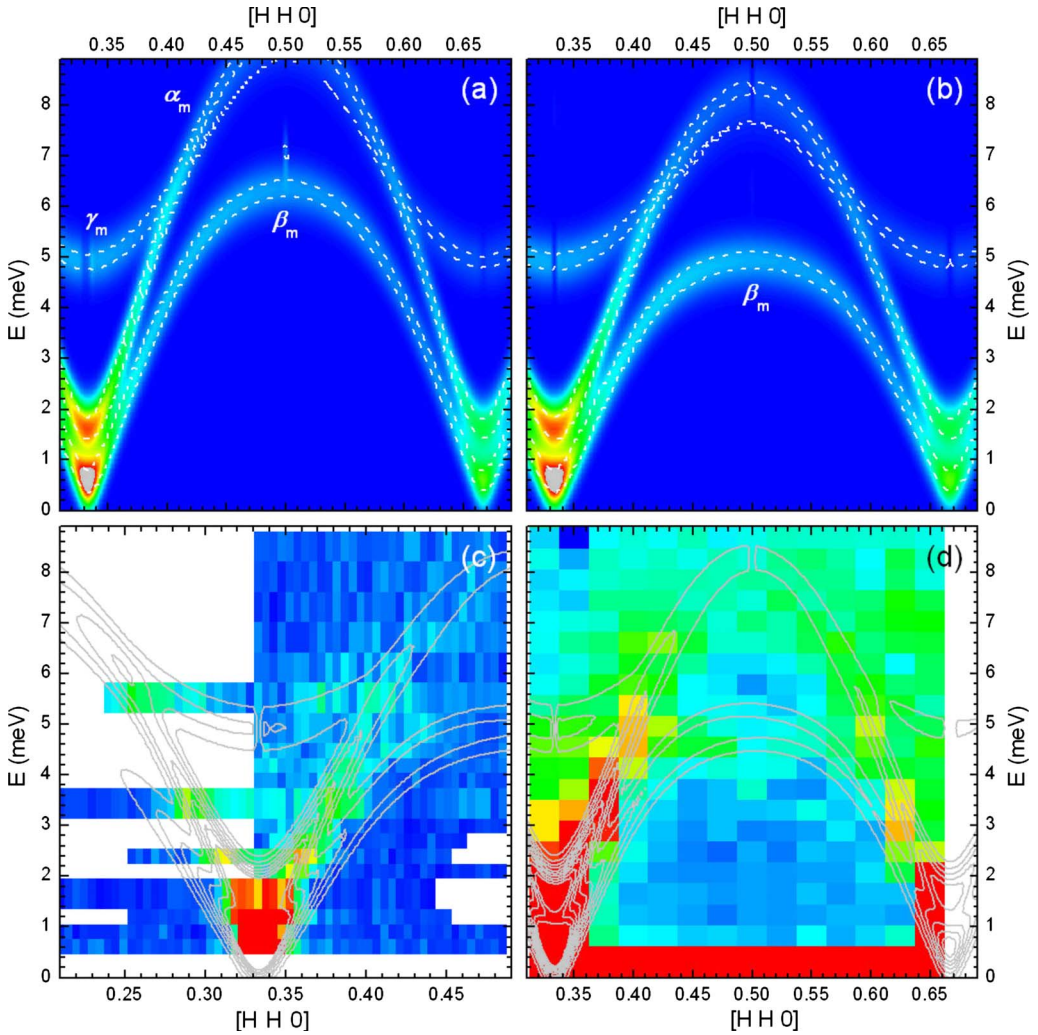

FIG. 6. (Color online) Calculated dynamical structure factor of $CuCrO_2$, plotted versus wave vector $[H\ H\ 0]$ and energy transfer E, using Heisenberg Hamiltonian (5) in the case of the modulated helicoidal magnetic structure model (a) without J_{NN} and (b) with an additional J_{NN} coupling term (see text). The different spin-wave modes are outlined in white. [(c) and (d)] Superimposition of the calculated model (dark gray lines) on the experimental inelastic scattering data map at 10 K recorded at k_f=1.550 and 1.970 $Å^{-1}$, respectively.

Scattering profiles along the $[H\ H\ L]$ directions are illustrated in Fig. 7(a), which shows data taken at fixed energy E=2.5 meV, as a function of H, for a number of L values. We observe that the peak positions are only weakly L dependent, demonstrating that the coupling J_c between the planes is extremely weak. This result is fully consistent with the observation of very broad magnetic Bragg peaks at 1.5 K,[8] which was interpreted as short-range (~200 Å) magnetic correlations along c, resulting from a weak interplane coupling. Examples of the profiles calculated for different values of J_c are illustrated in Fig. 7(b). It is not possible to determine the sign of J_c or estimate its value within the accuracy of the results, however, we nevertheless can approximate the bandwidth of the dispersion along the c direction in the range $[-0.2, 0.2]$ meV, which corresponds to $-0.1 < J_c/J_{ab} < 0.1$ in the phase diagram of Fig. 2.

With the available experimental data, it is actually quite difficult to decide which model describes $CuCrO_2$ best. The modulated helicoid should provide in theory the closest description, but it does not reproduce exactly the softening of the spin-wave mode around $(\frac{1}{2}\ \frac{1}{2}\ 0)$, and probably leads to an underestimation of J_{NN} in the calculation. Both models still remain fairly simple, as they do not take into account the magnetic incommensurability, but both also give consistent values of the magnetic couplings. Even though we are unable to determine the nature or strength of the interplane coupling J_c from the experimental dispersion along c, inelastic scattering data in the ab plane clearly indicate that next-nearest-neighbor coupling J_{NN} is not negligible in $CuCrO_2$: it is antiferromagnetic, and can be estimated to range between 0.1–0.25 meV depending on the chosen model. This is quite an unforeseeable result, which only inelastic scattering could evidence.

The modeling parameters obtained from the inelastic scattering study can now be compared with the theoretical calculations summarized in Fig. 2. Using J_{ab}=2.30 meV from the INS modeling of the magnetic structure, this leads, for the nonmodulated (modulated) models to $J_{NN}/J_{ab} \sim 0.108$ (0.052). It is rather straightforward to see, according to the classical energy calculations, that, if $J'_{ab}/J_{ab}=1$, a weak fer-

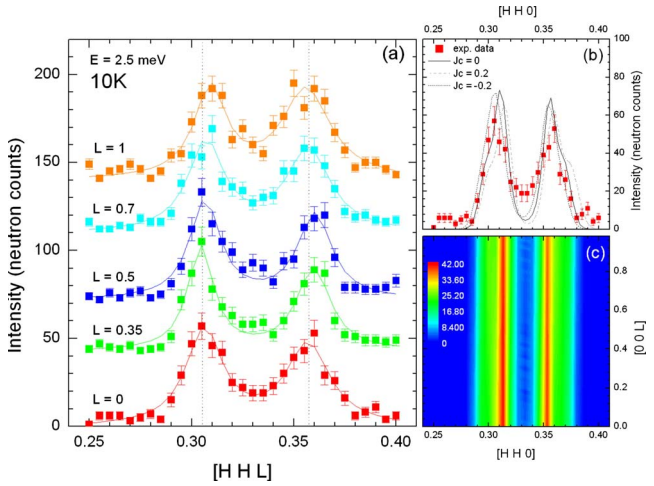

FIG. 7. (Color online) Inelastic neutron-scattering study along $[H\ H\ L]$ (k_f=1.550 Å^{-1}). (a) Spin-wave excitation scans at constant energy transfer (E=2.5 meV) along the $[H\ H\ L]$ directions (L=0,0.35,0.5,0.7,1). Data are shifted for clarity. (b) Comparison between experimental and modeled dispersion profiles along $[H\ H\ 0]$ calculated for different values of interplanar coupling J_c =0, 0.2, and −0.2 meV in the modulated helicoid case. (c) Intensity contour of the calculated dispersion in the $[H\ H\ L]$ plane (E =2.5 meV), for a ferromagnetic interplanar coupling J_c= −0.08 meV in the modulated helicoidal structure case.

romagnetic coupling is needed to stabilize a structure with q=0.329 [Fig. 2(a)]. In that case J_c can be estimated using Eq. (3) to be ∼−0.04 (−0.08) meV [illustrated as an empty (filled) star in the phase diagram of Fig. 2(a)]. As an example, the dispersion calculated in the case of the modulated helicoid model for J_{ab}=J'_{ab}=2.30 meV, J_c=−0.08 meV, and $D_{(110)}$=0.40 meV, is illustrated in Fig. 7(c) and is in good agreement with the data. However, with the J_{NN} value deduced from INS measurements, it also follows that, as soon as $J'_{ab}/J_{ab}>1.02$, the q=0.329 structure of $CuCrO_2$ can be stabilized for a tenuous antiferromagnetic J_c. As a result, not knowing the exact value of J'_{ab}/J_{ab} in $CuCrO_2$ prevents any actual insight on the sign of the interplane coupling J_c: whatever the chosen model, the helicoidal magnetic structure of $CuCrO_2$ is stabilized by a weak antiferromagnetic next-nearest-neighbor coupling [J_{NN}=0.25 (0.12) meV], in addition to a weak interplane coupling $-0.2<J_c<0.2$ meV, whose value will depend on J'_{ab}/J_{ab}. Because of this significant value of J_{NN}, the helicoidal structure of $CuCrO_2$ actually lies very close to the limit of stability of the collinear magnetic phase.

IV. DISCUSSION

In $CuCrO_2$, calculations and experimental observations have thus highlighted the delicate balance between J'_{ab}/J_{ab}, J_{NN}, and J_c to stabilize the incommensurate helicoidal magnetic order. An improved model is, however, required to further understand some of the more subtle features of the inelastic scattering data. Very few studies of the spin dynamics in other transition metal (TM) delafossite compounds are actually available in the literature and they mainly concern undoped and Al-doped $CuFeO_2$. Ye *et al.*, in Ref. 13, described the spin dynamics in the collinear four-sublattice structure of $CuFeO_2$ using a $J_{ab}\sim1.14$ meV, a strong J_{NN} ~0.50 meV, and an additional next-next-nearest-neighbor coupling $J_{NNN}\sim0.65$ meV, though the authors themselves acknowledge that there are no really clear physical grounds to it. In $CuFeO_2$, the excitation along c is also clearly dispersive, and the interplane coupling is accordingly strongly antiferromagnetic ($J_c\sim0.33$ meV). A quantitative analysis of the magnetic couplings in $CuFeO_2$ is beyond the scope of this paper, but we note that, in a fairly broad interpretation of our ENERMAG calculations, larger coupling values will lead to a larger deviation from commensurability, and for a strong J_{NN} coupling, to a collinear phase, in agreement with what is observed for $CuFeO_2$. A more detailed INS investigation of other TM delafossites is required at this point to draw a general picture, but the relative strengths of the magnetic paths J_{ab}, J_{NN}, and J_c dictated by the structural topology are certainly strongly dependent on the TM element. The strength of the interplane coupling J_c, intermediated by the linear copper bonding, seems, in particular, to depend highly on the nature of the TM cation.

Ye *et al.* also point out that, even if the collinear structure of $CuFeO_2$ shows magnetic Bragg reflections at $(\frac{1}{4}\ \frac{1}{4}\ \frac{3}{2})$, the dispersion exhibits two minima at the Q positions corresponding to the two incommensurate magnetic Bragg peaks positions. Indeed, the main difference between the spin dynamics in the collinear phase of $CuFeO_2$ and the incommensurate phase of $CuFe_{1-x}Al_xO_2$ (x=0.0155) lies in the low-energy part of the spectrum, where it can be seen that the energy of the spin-wave modes at these particular Q vectors softens down to zero.[22] The spin dynamics in both structures is thus very similar, and it is plausible that the spin Hamiltonian remains basically identical. Based on these considerations, it seems that the transition toward the collinear four-sublattice magnetic phase in $CuFeO_2$ is not purely an effect of magnetic coupling, but is rather related to an additional interaction, likely to be a strong coupling to the lattice in this case. In this sense, the substantial J_{NN} value, coupled to a significant spin-lattice effect, could be understood as the driving force triggering the symmetry lowering transition in $CuFeO_2$. In $CuCrO_2$, although a J_{NN} coupling has been evidenced, it has a smaller amplitude than in $CuFeO_2$. Accordingly, hints to a possible magnetoelastic coupling can be seen in the subtle relaxation of the compression along c of the CrO_6 octahedron[8] and the contraction of the crystallographic axis normal to the helicoid plane[9] at the onset of spin ordering.

Interestingly, the stabilization of the four-sublattice collinear magnetic structure to the detriment of the incommensurate one in $CuFeO_2$ coincides with the disappearance of the multiferroic behavior. In contrast, $CuCrO_2$, with weak J_{NN} and J_c, is multiferroic below T_N and remains down to the lowest temperatures a good example of an almost perfect 2D Heisenberg system on a triangular lattice. The transition at finite temperature toward a 3D magnetically ordered state, concomitantly with a ferroelectric phase, is only ensured by the small perturbations J'_{ab}/J_{ab}, J_{NN}, and J_c.

V. CONCLUSION

In summary, the spin dynamics of the geometrically frustrated triangular antiferromagnet multiferroic $CuCrO_2$ has been mapped out using inelastic neutron scattering. We have determined the relevant spin Hamiltonian parameters, showing that the helicoidal model with a strong planar anisotropy correctly describes the spin dynamics. The weakly dispersive excitation along *c* reflects the 2D character of the magnetic interactions, but the spin dynamics in $CuCrO_2$ clearly point out the relevance of the next-nearest-neighbor interaction to stabilize the magnetic order.

ACKNOWLEDGMENT

Financial support for this work was partially provided by the French Agence Nationale de la Recherche, Grant No. ANR-08-BLAN-0005-01.

*Corresponding author; sylvain.petit@cea.fr

[1] T. Kimura, J. C. Lashley, and A. P. Ramirez, Phys. Rev. B **73**, 220401 (2006).
[2] S. Seki, Y. Onose, and Y. Tokura, Phys. Rev. Lett. **101**, 067204 (2008).
[3] N. Terada, S. Mitsuda, H. Ohsumi, and K. Tajima, J. Phys. Soc. Jpn. **75**, 023602 (2006).
[4] S. Mitsuda, N. Kasahara, T. Uno, and M. Mase, J. Phys. Soc. Jpn. **67**, 4026 (1998).
[5] F. Ye, Y. Ren, Q. Huang, J. A. Fernandez-Baca, P. C. Dai, J. W. Lynn, and T. Kimura, Phys. Rev. B **73**, 220404 (2006).
[6] M. F. Collins and O. A. Petrenko, Can. J. Phys. **75**, 605 (1997).
[7] H. Kadowaki, H. Kikuchi, and Y. Ajiro, J. Phys.: Condens. Matter **2**, 4485 (1990).
[8] M. Poienar, F. Damay, C. Martin, V. Hardy, A. Maignan, and G. André, Phys. Rev. B **79**, 014412 (2009).
[9] K. Kimura, T. Otani, H. Nakamura, Y. Wakabayashi, and T. Kimura, J. Phys. Soc. Jpn. **78**, 113710 (2009).
[10] H. Yamaguchi, S. Ohtomo, S. Kimura, M. Hagiwara, K. Kimura, T. Kimura, T. Okuda, and K. Kindo, Phys. Rev. B **81**, 033104 (2010).
[11] K. Kimura, H. Nakamura, S. Kimura, M. Hagiwara, and T. Kimura, Phys. Rev. Lett. **103**, 107201 (2009).
[12] T. H. Arima, J. Phys. Soc. Jpn. **76**, 073702 (2007).
[13] F. Ye, J. A. Fernandez-Baca, R. S. Fishman, Y. Ren, H. J. Kang, Y. Qiu, and T. Kimura, Phys. Rev. Lett. **99**, 157201 (2007).
[14] M. Soda, K. Kimura, T. Kimura, M. Matsuura, and K. Hirota, J. Phys. Soc. Jpn. **78**, 124703 (2009).
[15] K. Kimura, H. Nakamura, K. Ohgushi, and T. Kimura, Phys. Rev. B **78**, 140401 (2008).
[16] M. Poienar, C. Martin, A. Maignan, and V. Hardy (unpublished).
[17] N. El Khayati, R. C. El Moursli, J. Rodriguez-Carvajal, G. Andre, N. Blanchard, F. Bouree, G. Collin, and T. Roisnel, Eur. Phys. J. B **22**, 429 (2001).
[18] D. H. Lyons and T. A. Kaplan, Phys. Rev. **120**, 1580 (1960).
[19] M. J. Freiser, Phys. Rev. **123**, 2003 (1961).
[20] H. Kadowaki, H. Takei, and K. Motoya, J. Phys.: Condens. Matter **7**, 6869 (1995).
[21] H. Kawamura, Prog. Theor. Phys. **101**, 545 (1990).
[22] N. Terada, S. Mitsuda, T. Fujii, and D. Petitgrand, J. Phys.: Condens. Matter **19**, 145241 (2007).